Engineering of 3D printed personalized polypills for the treatment of the metabolic syndrome

Brayan J. Anaya[1#], José Cerda[1#], Rita Datri[1], I. Yuste [1], F.C. Luciano [1], Aytug Kara[1], Helga K. Ruiz[2*], M.P. Ballesteros[1,3], D.R. Serrano [1,3*]

[1] Pharmaceutics and Food Technology Department, Faculty of Pharmacy, Universidad Complutense de Madrid, Plaza Ramón y Cajal s/n, 28040 Madrid, Spain.

[2]Department of Physical Chemistry, Complutense University of Madrid, 28040 Madrid, Spain

[3]Instituto Universitario de Farmacia Industrial, Faculty of Pharmacy, Universidad Complutense de Madrid, 28040, Madrid, Spain.

First coauthorship shared

*Corresponding authors

Dolores R Serrano – drserran@ucm.es

Helga K. Ruiz – helgakar@ucm.es

Abstract

Metabolic syndrome is a collection of abnormalities, including at least three of the following insulin resistance, hypertension, dyslipidemia, type 2 diabetes, obesity, inflammation, and non-alcoholic fatty liver disease. 3D printed solid dosage forms have emerged as a promising tool enabling the fabrication of personalized medicines and offering solutions that cannot be achieved by industrial mass production. Most attempts found in the literature to manufacture polypills for this syndrome contain just two drugs. However, most fixed-dose combination (FDC) products in clinical practice required the use of three or more drugs. In this work, Fused deposition modelling (FDM) 3D printing technology coupled with Hot-melt extrusion (HME) has been successfully applied in the manufacture of polypills containing nifedipine (NFD), as an antihypertensive drug, simvastatin (SMV), as an antihyperlipidemic drug, and gliclazide (GLZ) as an antiglycemic drug. Hanssen solubility parameters (HSPs) were utilized as predictors to guide the formation of amorphous solid dispersion between drug and polymer to ensure miscibility and enhanced oral bioavailability. The HSP varied from 18.3 for NFD, 24.6 for SMV, and 7.0 for GLZ while the total solubility parameter for the excipient mixture was $27.3^{0.5}$. This allowed the formation of an amorphous solid dispersion in SMV and GLZ 3D printed tablets compared to NFD which was partially crystalline. Popypill showed a dual release profile combining a faster SMV release (< 6 h) with a 24 h sustained release for NDF and GLZ. This work demonstrated the transformation of FDC into dynamic dose-personalized polypills.

Keywords: 3D Printing, fused deposition modelling (FDM), nifedipine, simvastatin, gliclazide; polypill, personalized medicines.

Graphical Abstract

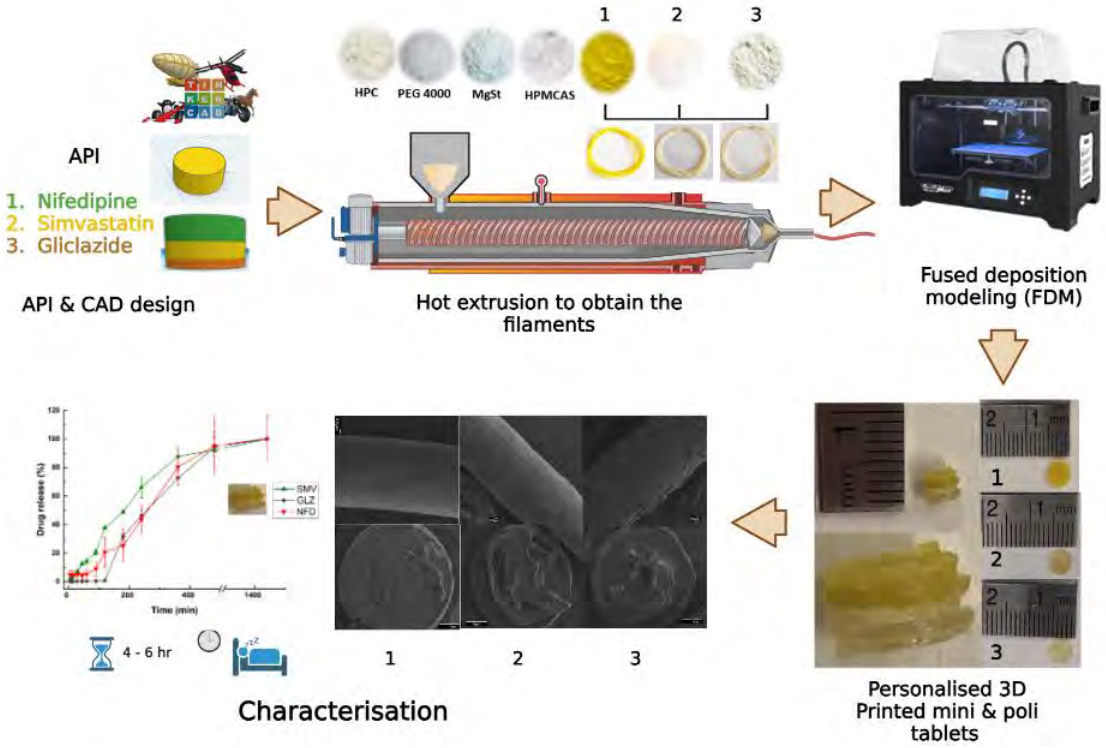

1. Introduction

Metabolic syndrome is a collection of abnormalities, including at least three of the following insulin resistance, hypertension, dyslipidemia, type 2 diabetes, obesity, inflammation, and non-alcoholic fatty liver disease [1]. It is fast becoming a major global health challenge, because of high mortality and morbidity. For this reason, a wide variety of resources are invested to stop the spread of this syndrome considering that better control might help to prevent sarcopenia, strokes, heart attack, and diabetic coma [2].

Personalized medicine generally consists in tailoring medical treatments to the characteristics, needs, and preferences of every single patient, and it involves purposely running diagnosis, therapy, and follow-up [3]. Personalized medicine can be defined as "Providing the right treatment to the right patient, at the right dose, at the right time" [4, 5]. Indeed, the goal of personalized medicine is to drive clinical decision-making by distinguishing in advance those patients who are most likely to benefit from a given treatment from those who would incur costs and side effects without gaining equivalent benefits. The multiple benefits of treatment personalization are evident, the more remarkable being the reduction of side effects and the maximization of the efficiency and effectiveness of the use of medicinal resources [6].

3D printed solid dosage forms have emerged as a promising tool enabling the fabrication of personalized medicines and offering solutions that cannot be achieved by industrial mass production [7, 8]. Several clinical trials are already in progress to demonstrate the successful implementation of 3D printed medicines in hospital settings [9]. An additional advantage of 3D printing manufacturing is their versatility to manufacture Fixed-Dose Combination (FDC) products, those that contain two or more Active Pharmaceutical Ingredients (API), which is especially useful for polymedicated patients that suffer from diabetes, hypertension, and hypercholesterolemia [10]. FDC medicines have increasingly attracted the attention of both patients and clinicians, due to a multitude of benefits such as improved patient compliance and more convenient dosing associated with improved clinical performance. However, manufacturing safe, efficient, and effective FDC medicines is not an easy task at the industrial level due to segregation issues during mixing processes, physicochemical interactions between APIs, and the need for different drug release profiles within the same

solid dosage form. Also, the range of doses and API combinations is limited at the industrial level. 3D printing can overcome the abovementioned challenges associated with the manufacturing of complex FDCs. Several 3D printed techniques are currently under research to enable fast and high-quality manufacturing of FDC medicines [11]. Nozzle-based extrusion systems, such as fuse deposition modeling (FDM) and pressure-assisted microsyringes (PAM), laser-based systems such as stereolithography (SLA), and powder bed fusion techniques such as selective laser sintering (SLS) are the most promising techniques till now [12-14].]. The main two advantages of FDM over laser-based printing techniques are the feasibility of using pharmaceutical-grade excipients to manufacture tablets unlike photopolymerizable resins and photoinitiators materials required for SLA and SLS being required further toxicological studies to guarantee the safety after chronic use of these excipients. Additionally, FDM does not require a post-printing step while this is mandatory for other techniques such as SLA and PAM to ensure the full removal of unpolimerized residues and solvents, and also, FDM provides high mechanical strength which can be difficult to achieve for PAM-fabricated tablets [8].

However, polypill fabrication using FDM 3D printing technology is challenging as passive diffusion results in poor drug loading capacity, being 4% one of the highest values reported in the literature~~. Passive drug diffusion across solid dosage forms previously prepared by FDM has been optimized reaching up to 4% drug loading efficiencies~~ [15]. ~~However,~~ FDM coupled with hot-melt extrusion (HME) has been shown to possess one of the greatest versatility to manufacture FDC formulations with high drug loading capacity and excellent mechanical strength properties as well as unlimited geometries that can be printed resulting in greater control of drug release [16], but deep knowledge of the critical material attributes is essential to manufacturing optimal filaments for ready-to-use FDM printers as well as understanding the polypill design to avoid physicochemical interactions and to achieve the desired drug release profile. Despite the potential use of polypills containing three or more drugs to treat metabolic syndrome to enhance patient compliance, the number of successfully printed polypills using FDM is very limited due to the complexity of the manufacturing process [17-20]. More studies are required combining different active ingredients and pharmaceutical-grade excipients to enable the transformation of FDC into dynamic dose-personalized polypills in the near future [21].

The hypothesis underpinning this work is that FDM coupled with HME could be easily translated into clinical practice such as hospital and community pharmacies for the treatment of metabolic syndrome combining drugs with different release profiles if filaments prepared by HME are provided to professional healthcare providers. A versatile platform technology that combines 3D printing, HME, and control API release would result in a feasible approach to implementing 3D printing polypills for metabolic syndrome in clinical settings. A proof of concept has been demonstrated by manufacturing individual filaments containing different BCS Class II drugs such as nifedipine, a calcium-channel blocker to reduce blood pressure, simvastatin, an antihyperlipidemic drug and gliclazide, a second-generation sulfonylurea used as a hypoglycemic drug for treating non-insulin-dependent diabetes mellitus. Those filaments were combined either in single API tablets or within polypills. A full characterization of 3D printed pill physicochemical performance was carried out.

2. Material and methods

2.1. Materials

Nifedipine (NFD) was purchased from Industria Chimica Italiana (>95%, Bergamo, Italy). Gliclazide (GLZ) was purchased from Kemportec Limited (>98%, Cornforth, UK). Simvastatin (SMV), polyethylene (PEG) 4000, and magnesium stearate were purchased from Sigma-Aldrich (Madrid, Spain). Hypromellose acetate succinate (HPMCAS) (AQOAT® LG grade) was a gift from Shin-Etsu (Tokyo, Japan). Klucel hydroxypropyl cellulose (HPC, 95 kDa) LF grade was kindly donated by Ashland (Madrid, Spain). Solvents were HPLC grade and were purchased from Proquinorte (Madrid, Spain). Any other reagents were used without further purification and were of analytical grade.

2.2. Methods

2.2.1. Preparation of filaments

Each of the APIs (NFD, SMV, and GLZ) at 50% was mixed with the following excipients, PEG 4000 (7.5%), HPC (5%), HPMCAS (36.5%), and magnesium stearate (1%) using a ball milling (IKA Ultra-Turrax® Tube Drive Disperser) to blend the feed powder mixture for 2 min at 6000 rpm after which the mixture was sieved through a 12-US mesh (1.68 mm) screen before extrusion to ensure homogenous particle size and minimize the risk for segregation. HPC and HPMCAS were used to create a modified-release polymeric matrix. PEG 4000 was

included as a plasticizer, and magnesium stearate as a lubricant to promote the homogenous transit of the powder mixture inside the hot-melt extruder. HME of the mixture was performed with a Noztek touch single-screw extruder (Shoreham, UK) at 30 rpm using a 2 mm die. A 20 g batch size was used. NFD filaments were extruded at 160 ºC, SMV at 135 ºC, and GLZ at 145 ºC. After printing, filaments were protected from light with foil and were stored under desiccated conditions, to avoid drug degradation and filament hydration until further analysis was performed.

2.2.2. Geometry design and 3D printing settings

The tablet geometry was designed using computer-aided design (CAD) software (Tinkercad®) and was exported into a standard tessellation language (.stl) digital file. The .stl file was imported into Ultimaker Cura (Ultimaker B.V.®, Utrecht, The Netherlands) for slicing into to g-code file format for FDM printing. Bearing in mind the density of the filaments (1.25 ± 0.2 g/cm^3) and the drug loading required in each filament, rounded flat tablets were designed to contain 20 mg of NFD, 10 mg of SMV, and 10 mg of GLZ of 5 mm in width and with different heights of 1.5 mm, 1 mm, and 1 mm for NFD, SMV, and GLZ respectively. A combined polypill was also designed consisting of three cylindrical sections of 50% NFD, 33.3% SMV, and 16.6% GLZ of the total volume, with a total height of 3.2 mm.

The Anycubic Mega Zero FDM printer with 0.1 mm layer resolution, 0.125 mm XY resolution, and 0.4 mm nozzle diameter was used for printing the filaments of NFD, SMV, and GLZ. Layer height was set to 0.1 mm for achieving high resolution and the printer head followed a geometric pattern with a 30 mm/s speed while printing and 30 mm/s while traveling. The infill was set at 100% and a total number of 28 layers were printed for the combined polypill. The individual tablets contained 12 layers for NFD, 8 for SMV, and 8 for GLZ. The printing temperature was 160 ºC for NFD, 140 ºC for GLZ, and 155 ºC for SMV.

2.2.3. Physicochemical and solid state characterisation of filaments and tablets

Tablet mass uniformity and dimensions

Tablets (n = 10) were weighed in an analytical balance to compare the mass deviation between the printed dosage forms for each API. The dimensions were measured with a caliper (Cole Parmer, Fisher Scientific, Madrid, Spain). The coefficient of variation (CV) was also

calculated ~~as the ratio of the standard deviation, and the average mean value of each parameter multiplied by 100~~ [22].

Imaging

To evaluate the shape, the surface morphology of the printed tablets, and validate the dimensions, a digital microscope (U500X, CoolingTech, Shenzhen, China) was used and images were processed by ImageJ v1.46 image analysis software (University of Wisconsin, Madison, WI, USA). To gather a more in-depth analysis of the morphology of the tablets and filaments at different stages of the experimental process, a Scanning Electron Microscope (JSM 6335F JEOL, Japan) equipped with a secondary electron detector at 15 kV was used after the samples were sputter coated with pure gold using a metallizer (Q150RS Metalizador QUORUM, Quorum Technologies Ltd., Lewes, UK) for 180 s under vacuum. Micrographs were obtained from filaments, 100% fully printed tablets, APIS raw material, and excipients used.

Powder X Ray Diffraction (PRXD)

Powder X-ray analysis was carried out using a Philips®X'Pert-MPD X-ray diffractometer (Malvern Panalytical®; Almelo, The Netherlands) equipped with Ni-filtered Cu K radiation (1.54). A 40 kV voltage and 40 mA current were used to perform the study. PXRD patterns were recorded at a step scan rate of 0.05° per second from 5° to 40° on the 2-theta scale (n = 3). Physical mixtures of raw powder materials between API and excipients were carried out in an agate mortar and pestle for comparison purposes.

Fourier-Transform Infrared (FTIR) Spectroscopy

FTIR analysis was carried out with a Nicolet Nexus 670–870 (Thermofisher, Madrid, Spain). A wavelength range between 400–4000 cm^{-1} was used. Spectragryph (version 1.2.9, Oberstdorf, Germany) software was used for the interpretation of the spectra. Data normalization was performed [23].

Differential Scanning Calorimetry (DSC)

DSC-TGA Standard scans were performed using nitrogen as the purge gas on a SDT Q600 instrument (TA instruments, Elstree, UK) calorimeter. A scanning rate of 10 °C/min was used from room temperature up to 200 °C. The instrument was calibrated using indium as the standard.

To calculate the degree of crystallinity (Xc) of the API within the amorphous solid dispersion, equation (1) was used:

$$Xc\ (\%) = [(\Delta Hf_{SD})/\Delta Hf_{PM}) \times 100 \quad (1)$$

Where ΔHf_{PM} was considered as the heat of fusion of the drug within the physical mixture and ΔHf_{SD} the heat of fusion of the drug within the solid dispersion [24].

2.2.4. Hanssen Solubility parameters calculation

The total solubility parameter, δt , represents the total attractive forces in a condensed matter and can be expressed as the square root of the sum of Hansen solubility parameters (HSPs) according to equation 2:

$$\delta t = (\delta d^2 + \delta p^2 + \delta h^2)^{0.5} \quad (2)$$

where δ_d accounts for the dispersion forces, δ_p for the polar forces, and δ_h for hydrogen-bonding attraction. HSPs were calculated according to the group contribution method [25, 26].

2.2.5. Dissolution Studies and release kinetic comparison

The dissolution tests were performed in triplicate to evaluate the release profile of tablets using a United States Pharmacopoeia (USP) apparatus 2 (ERWEKA DT 80, Heusenstamm, Germany). A stirring speed of 100 rpm was utilised to investigate the drug release profile ~~under stressed conditions~~. The dissolution media was USP simulated gastric fluid (SGF) without enzymes (pH 1.2) containing 2 g of sodium chloride (NaCl), and 7 mL of hydrochloric acid (HCl, 37%) per liter of deionised water with 0.5% sodium lauryl sulfate for the first two hours, followed by USP simulated intestinal fluid (SIF) without enzymes (pH 6.8) prepared using 6.8 g of monobasic potassium phosphate (KH2PO4) and 0.62 g of sodium hydroxide (NaOH) per liter of deionised water with 0.5% sodium lauryl sulfate, as described in the USP [27, 28]. SGF (250 mL) was used during the first 2 h. Afterward, SIF (250 mL) was added, and dissolution continued for 22 h at 37 ± 0.5 °C. NaOH (10 M) was used to adjust the pH to 6.8 after the addition of the SIF. Samples (2 mL) were withdrawn from the dissolution media and filtered through a hydrophilic 0.45 μm filter (Millipore, Millex-LCR, Merck, Madrid, Spain) at 5, 10, 15, 30, and 45 min, 1, 1.5, 2, 3, 4, 6, 8, and 24 h [23, 29]. Samples were diluted (1:1, v:v) with their corresponding mobile phase before analyses. As a comparison, the commercially available tablets were also tested, Nifedipine Adalat® OROS (30 mg), Simvastatin Normon® (20 mg), and Gliclazide Cinfa® (30 mg).

To investigate the release profile from the different commercial tablets and 3D printed formulations, the dissolution data obtained was fitted using the following kinetic equations: Zero Order (Equation 3), First order (Equation 4), Hixson–Crowell (Equation 5), Korsmeyer–Peppas (Equation 6) and Higuchi (Equation 7):

$$Q_t = Q_0 + K_{0t} \quad (3)$$

$$Q_t = \ln Q_0 + K_1 t \quad (4)$$

$$Q_\infty^{1/3} - (Q_\infty - Q_t)^{1/3} = K_s t \quad (5)$$

$$\frac{Q_t}{Q_\infty} = K_{KP} t^n \quad (6)$$

$$Q_t = KH\ t^{1/2} \quad (7)$$

where Q_t is the amount of drug dissolved in time t, Q_0 is the initial amount of drug in the solution (most times, $Q_0 = 0$), Q_∞ is the initial amount of drug in the tablet, $\frac{Q_t}{Q_\infty}$ is the fraction of drug release at time t, K_0 is the Zero-order release constant, K_1 is the first-order release constant, K_s is a constant incorporating the surface–volume relation, K_{KP} is a constant that describes the structural and geometric characteristics of the drug dosage form, KH is Higuchi constant and n is the release exponent that describes the drug release mechanism. To test the applicability of the drug release model, the regression coefficient (R^2) was used [30].

2.2.6. Quantification of NFD, SMV, and GLZ by High-Performance Liquid Chromatography (HPLC)

HPLC analysis was undertaken using modular Jasco equipment with a Jasco PU-1580 pump, a Jasco AS-2050-Plus autosampler fitted to a 100 µL sampling loop, and a UV-visible detector Jasco UV-1575. NFD, SMV, and GLZ were eluted on a Thermo Scientific ODS Hypersil C18 reverse-phase column (250 × 4.6 mm, 5 µm). NFD mobile phase consisted of methanol: water: acetonitrile (36:55:9 v/v). SMV mobile phase was consisting of acetonitrile: 0.1% H_3PO_4 aqueous solution (65:35 v/v) while GLZ mobile phase was consisting of phosphate buffer (KH_2PO_4 0.2 M, pH 4.4): acetonitrile: methanol (45:40:15 v/v/v). The mobile phases were filtered by a hydrophilic 0.45 µm filter (Millipore, Millex-LCR, Merck, Madrid, Spain), and pumped at a flow rate of 1 mL/min. The sample injection volume was

50 µL. The column temperature was kept at 25 °C and the detector was set at 240 nm for NFD, and 238 nm for SMV and GLZ.

2.2.7. Statistical Analysis

Statistical analysis for the dissolution study data was performed via a one-way ANOVA test using Minitab v.16 (Minitab Ltd., Coventry, UK) followed by Tukey's test (95% level of significance). The comparison and modeling of dissolution profiles were performed using the software DDsolver (China Pharmaceutical University, Nanjing, China). The dissolution results were plotted using Origin 2021 (OriginLab Corporation, Northampton, MA, USA).

3. Results

3.1. Manufacture of 3D-Printed tablets and filaments

The filaments prepared from different APIs (NFD, SMV, and GLZ) are shown in Figure 1. The extrusion process was successful even at high drug loading such as 50% for all three APIs. To optimize filament morphology, after the first extrusion cycle, the filament was cut into 1 mm in length sections which were extruded a second time at the same conditions for each API. The second extrusion allowed the elimination of bubble formation within the filament. The extruder was not equipped with a venting unit which did not allow air removal during the kneading and extruding process. The surface of NFD and SMV filaments was smooth and homogeneous while the visual appearance of GLZ filaments was rough and showed morphological defects and voids of around 100 µm (Fig 1C). The different printing and extrusion conditions were selected based on the melting point of each API (Table 2.). Temperature conditions were 10-20 ºC below the melting point of each drug to avoid drug degradation. The target diameter of the filaments was 1.75 mm. Filaments were pulled and winded which led to different diameter size reductions. The diameter of the different filaments obtained were 1.88 ± 7.9 mm, 1.51 ± 8.4 mm, and 1.99 ± 41.4 mm for NFD, SMV, and GLZ respectively. Changes in the morphology and the diameter in the filament have a critical impact on the dimension quality, weight, and uniformity of the final 3D printed tablets and, also unsuccessful printing or variations in the 3D printed process [31]. NFD showed the closest diameter size to 1.75 mm which translated in the printed tablets with the lowest weight variability. However, the differences in filament diameter for SMV and GLZ resulted in higher variations in the weight of the tablets (Table 1). Also, the variability in tablet height

for GLZ was greater than NFD and SMV which is related to the smaller dimensions of the tablets containing this API.

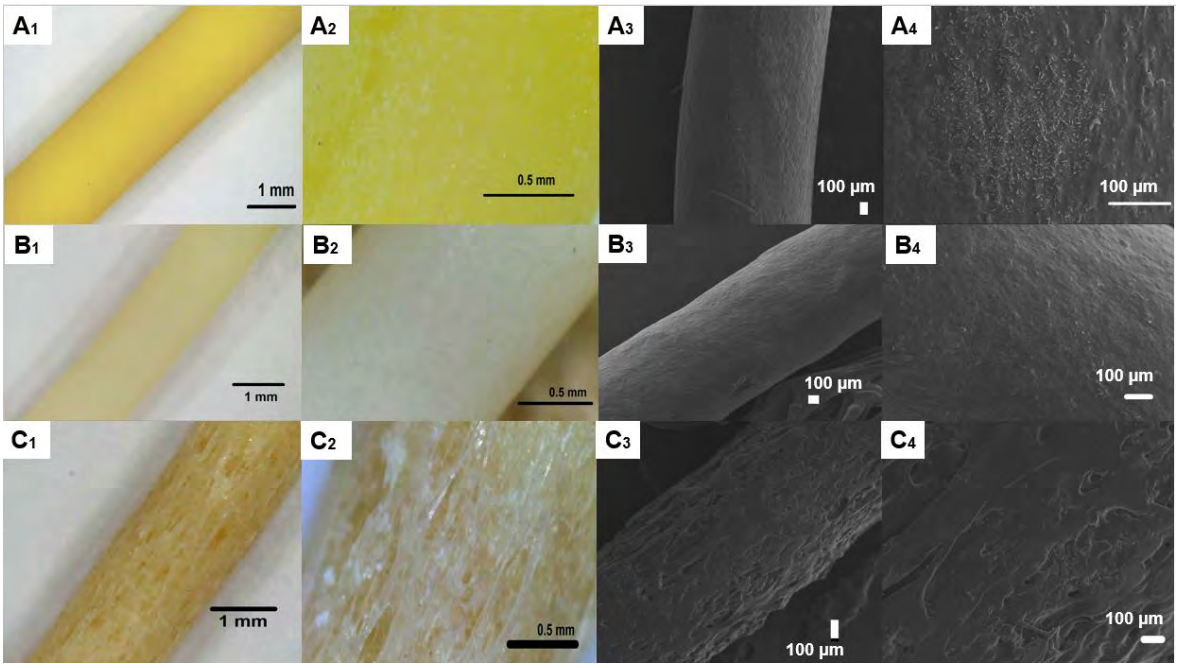

Figure 1. Morphological evaluation of single API filament. Key: **A**, NFD, **B**, SMV, **C**, GLZ. **A1, B1, C1** Images were obtained by a digital microscope at 50x magnifications; **A2, B2, C2** Images were obtained of the central surface of the filament obtained by a digital microscope at 300x magnifications; **A3, B3, C3** Micrographs were obtained by Scanning Electronic Microscopy at 30x magnifications; **A4, B4, C4** Micrographs were obtained by Scanning Electronic Microscopy at 100x magnification.

The 3D printed tablets were designed to contain 20, 10, and 10 mg of NFD, SMV, and GLZ respectively. Considering that the API drug loading was 50% for each API, the target tablet weight was 40 mg, 20 mg, and 20 mg for NFD, SMV, and GLZ respectively. In Table 1, the accuracy of printing is illustrated. Higher weight accuracy (> 99.8%) was obtained for NFD tablets with excellent mass uniformity for NFD (CV< 5%). Accuracy for printing SMV tablets was intermediate with an average weight of 114% of the target size and a CV of 27.9%. GLZ tablets showed the poorest printability properties. Tablet weight was 81.5% of the actual target and the CV was high (36.2%). This is highly dependent on filament characteristics. GLZ filaments showed voids which translated into a lack of deposited material and hence a much larger deviation from the target tablet dimensions.

Table 1. Mass and dimensions uniformity for the 3D printed tablets.

Drug	Tablet	Weight (mg)	Diameter (mm)	Height (mm)
NFD	Mean	39.9	5.65	1.54
	SD	1.3	0.08	0.05
	CV (%)	3.2	1.4	3.3
SMV	Mean	22.9	4.98	1.18
	SD	6.4	0.13	0.30
	CV (%)	27.9	2.6	25.4
GLZ	Mean	16.3	5.04	0.68
	SD	5.9	0.06	0.20
	CV (%)	36.2	1.2	29.4

No printing defects were visually detected in any of the 3D printed tablets; however, a rugous surface was observed in all the cases (Figure 2). NFD tablets showed a characteristic yellow transparent colour attributed to the NFD while SMV tablets showed a glass transparent colour which can indicate the formation of a solid solution after printing. In the case of GLZ tablets, an orangish colour was observed which may be attributed to partial drug degradation during printing.

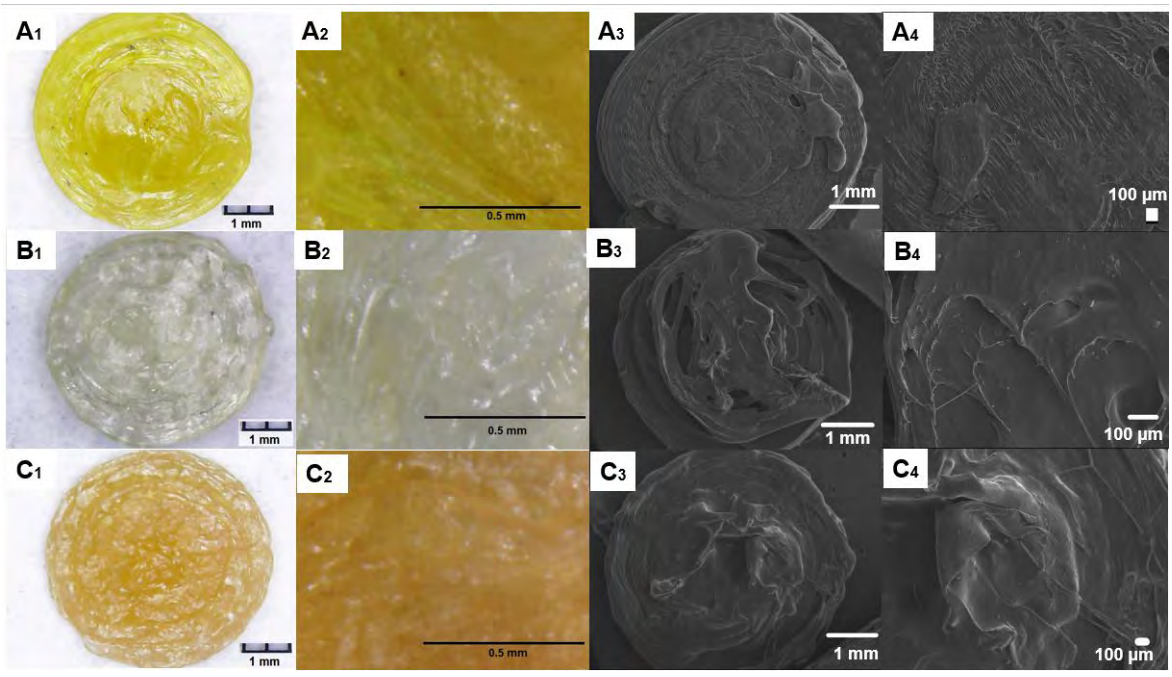

Figure 2. Morphological evaluation of single API 3D printed tablets. Key: A, NFD, **B**, SMV, **C**, GLZ. **A1, B1, C1** Images were obtained by a digital microscope at 50x magnifications; **A2, B2, C2** Images were obtained of the central top surface of the 3D printed tablet obtained by a digital microscope at 500 x magnifications; **A3, B3, C3** Micrographs were obtained by Scanning Electronic Microscopy at 20x magnifications; **A4, B4, C4** Micrographs were obtained by Scanning Electronic Microscopy at 50x magnification.

3.2. Solid-State Characterisation

Powder X-Ray Diffraction (PRXD)

The pXRD analysis of the unprocessed raw materials, 3D printed tablets, and filaments are illustrated in Figure 3. Significant differences were observed among the three APIs. NFD printed tablets showed a partially crystalline API as well as the extruded NFD filaments. The observed Bragg peaks matched those corresponding with the unprocessed drug and also PEG 4000 (Figure 3A). However, SMV tablets and filaments exhibited a characteristic amorphous halo which corresponds with the glassy transparency observed in the digital images (Figure 2B). In the case of the GLZ, the extruded filaments exhibited Bragg peaks attributed to the crystalline API but after printing, the drug was fully amorphized. Peaks observed in the GLZ 3D printed tablets are attributed to the PEG 4000 (Figure C).

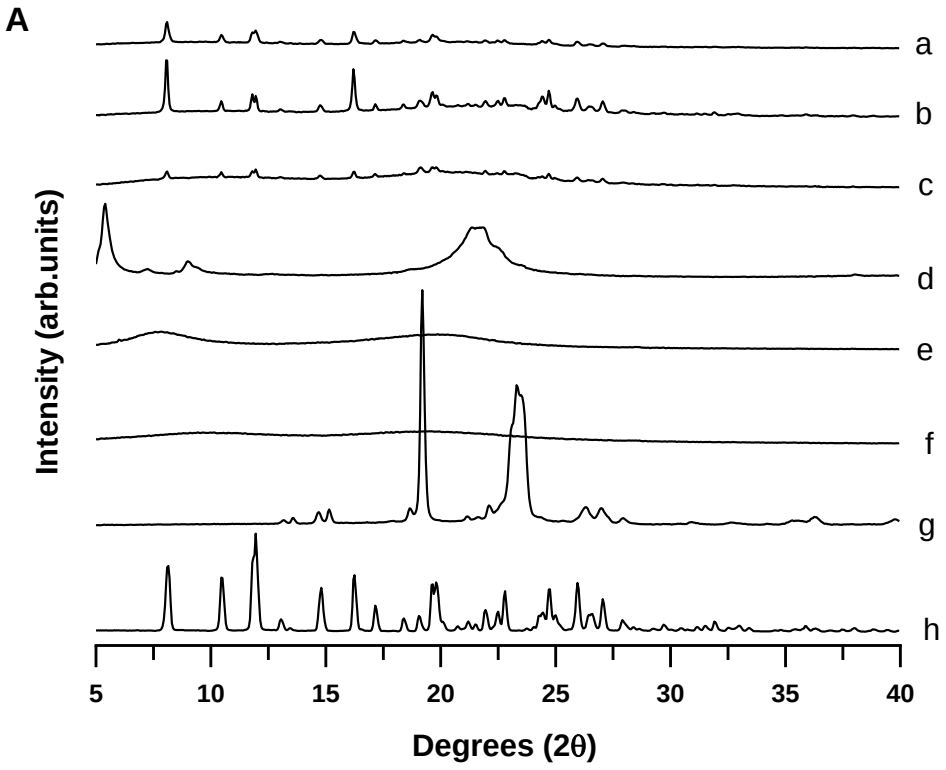

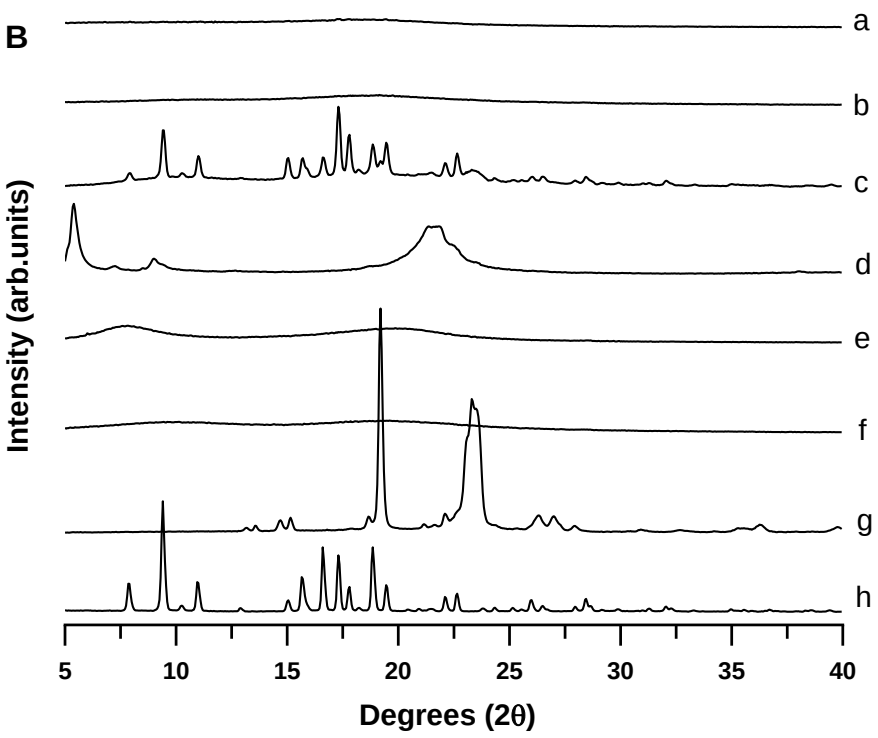
B
a
b
c
d
e
f
g
h
Intensity (arb.units)
5
10
15
20
25
30
35
40
Degrees (2θ)

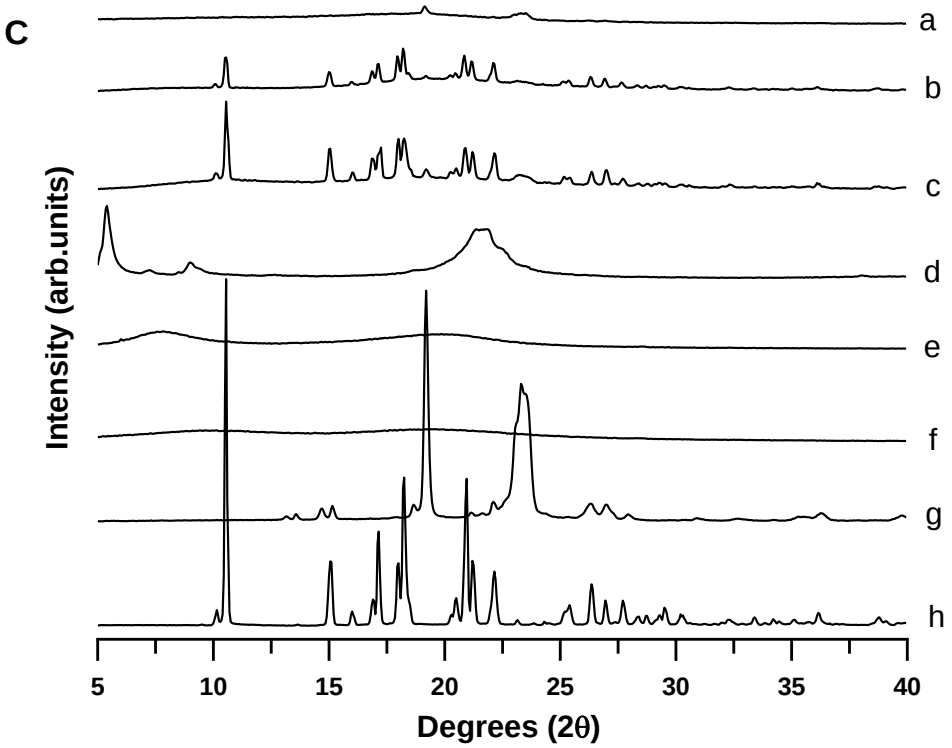
C
a
b
c
d
e
f
g
h
Intensity (arb.units)
5
10
15
20
25
30
35
40
Degrees (2θ)

Figure 3. **PXRD analysis for (A) NFD, (B) SMV, (C) GLZ formulations**. Key: (a) API 3D printed tablet, (b) Extruded filament, (c) Physical mixture, (d) Unprocessed magnesium stearate, (e) Unprocessed HPC, (f) Unprocessed HPMC, (g) Unprocessed PEG 4000, and (h) Unprocessed API.

Fourier Transform Infrared Spectroscopy (FTIR*)*

FTIR spectra showed clear hydrogen-bonding interactions between API and the excipients (Figure 4). Shifts were observed mainly in the carbonyl group (C=O) of the API matching the results obtained by PXRD. SMV showed the greatest shift in the C=O band from 1710 cm^{-1} in the raw material toward 1720 cm^{-1} in the filaments and 3D printed tablets. GLZ also showed a charactersitic shift in the C=O band from 1710 cm^{-1} toward 1718 cm^{-1}. This shift was observed only in the 3D printed tablets but not in the extruded filaments. The NFD formulations also exhibited a similar trend but with a smaller shift from 1682 cm^{-1} in the unprocessed NFD towards 1687 cm^{-1} in the process formulations.

Differential Scanning Calorimetry (DSC)

Unprocessed NFD, SMV, and GLZ showed a sharp endothermic event corresponding to the onset of the melting of the drug at 170.7 ± 2.1 ºC with a heat of fusion of 103.1 ± 1.1 J/g, 138.91 ± 1.7 ºC with a heat of fusion of 94.75 ± 0.7 J/g, and 168.72 ± 0.9 ºC with a heat of fusion of 131.3 ± 1.0 J/g for NDF, SMV, and GLZ respectively (Figure 5, Table 2). Unprocessed PEG 4000 also exhibited a sharp melting event at 61.35 ± 0.9 ºC with a heat of fusion of 317.4 ± 2.2 J/g (Figure 5). In all three formulations, a depression of the melting point of the API occurred for both extruded filaments and 3D printed tablets except for SMV tablets that did not exhibit any evidence of crystalline drug. The endothermic peak attributed to crystalline PEG 400 was observed in all the formulations except for those containing SMV. 3D printed tablets and filaments of SMV did not exhibit any endothermic peak related to the API or the PEG. Glass transition was not observed in any of the cases probably because the dehydration process occured at the same temperature obscuring the signal. Bearing in mind the enthalpy of fusion of the unprocessed NFD and the one observed in the tablet which contained 50% NFD, approximately fifty percent of the drug was crystalline while the rest was amorphized in the composite excipient blend. However, other authors have described a partial crystallization of the NFD during the DSC analyses [16]. In the case of GLZ, a similar trend was observed. Comparing the enthalpy of fusion of the unprocessed GLZ with the one

obtained for the drug in the 3D printed tablet, around 36% of the drug was found in the crystalline form. This result does not match those obtained in the XPRD which can be explained by the drug crystallization within the DSC analysis.

A

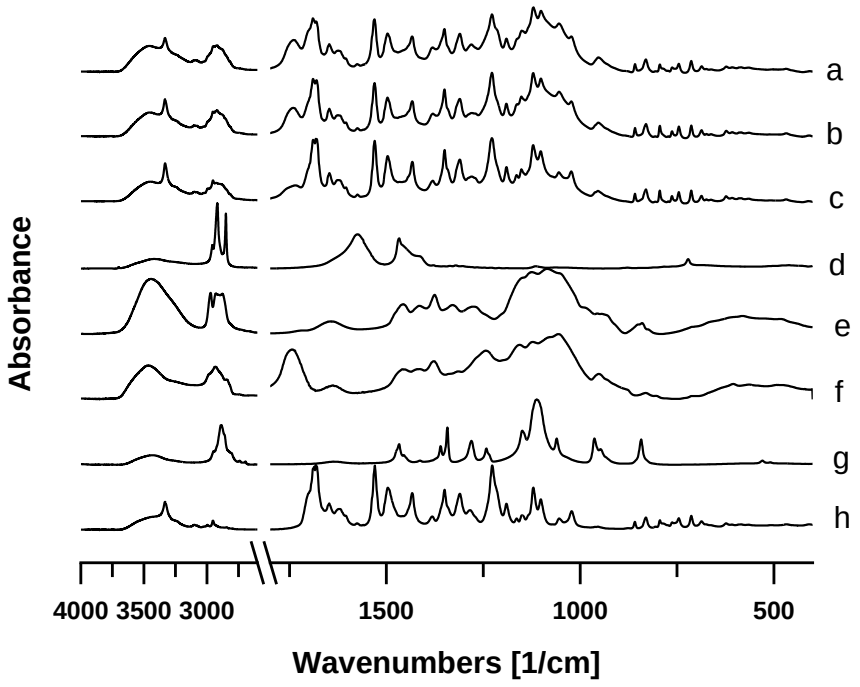

B

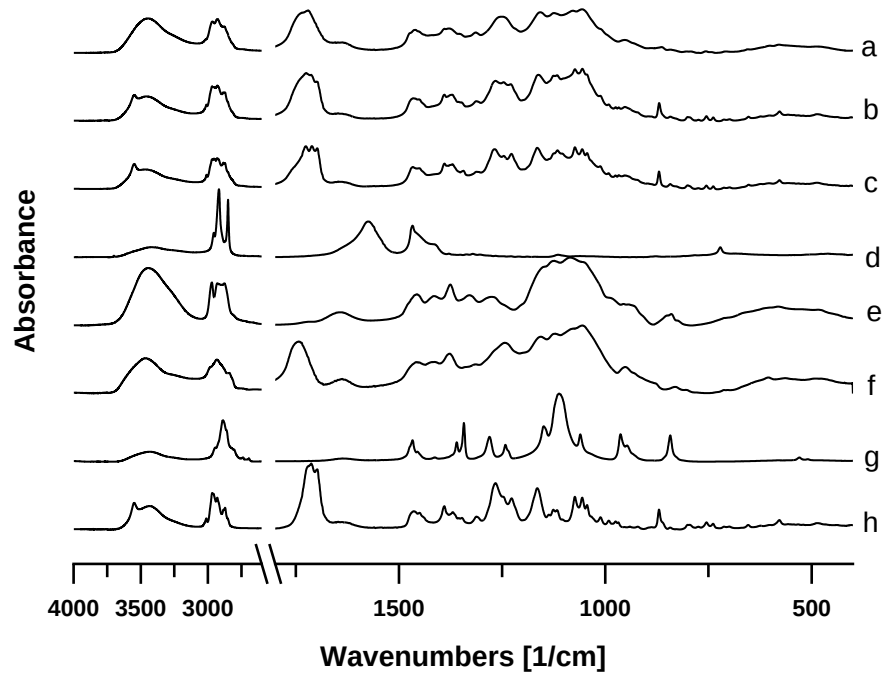
Absorbance
a
b
c
d
e
f
g
h
4000 3500 3000
1500
1000
500
Wavenumbers [1/cm]

C

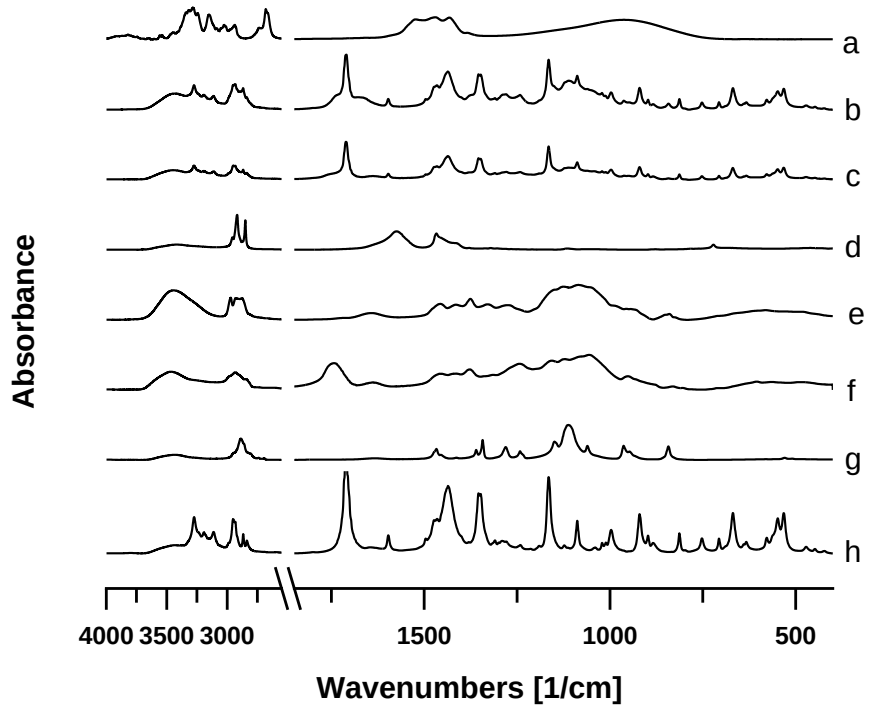
Absorbance
a
b
c
d
e
f
g
h
4000 3500 3000
1500
1000
500
Wavenumbers [1/cm]

Figure 4. F-TIR analysis for (A) nifedipine, (B) simvastatin, (C) gliclazide. Key: (a) API 3D printed tablet, (b) API filament, (c) Physical mixture, (d) Unprocessed magnesium stearate, (e) Unprocessed HPC, (f) Unprocessed HPMC, (g) Unprocessed PEG 4000, and (h) Unprocessed API.

Table 2. Enthalpy of fusion and melting events for APIs 3D printed tablets, filaments, physical mixtures, and unprocessed materials. Key: **ΔH_f,** heat of fusion**; Tm,** onset melting temperature**.**

Sample	**ΔH_f (J/g)**	**Tm (Onset) ($^{\circ}$C)**
NFD 3D printed tablets	114.4 ± 2.1	46.17 ± 0.7
	26.11 ± 0.2	159.02 ± 1.1
NFD Filament	91.39 ± 0.9	54.56 ± 0.9
	16.36 ± 1	158.61 ± 0.5
Physical Mixture NFD	91.06 ± 2	55.18 ± 2.5
	50.71 ± 2.4	164.09 ± 0.7
Raw NFD	103.1 ± 1.1	170.7 ± 2.1
SMV 3D printed mini-tablets	85.76 ± 0.4	51.62 ± 0.8
	-	-
SMV Filament	65.30 ± 0.3	42.81 ± 1.1
	-	-
Physical Mixture SMV	102.3 ± 2.7	58.54 ± 2.7
	43.68 ± 1.3	128.39 ± 3.0
Raw SMV	94.75 ± 0.7	138.91 ± 1.7
GLZ 3D printed mini-tablets	51.08 ± 1.7	50.89 ± 0.5
	24.50 ± 0.2	135.86 ± 0.4
GLZ Filament	84.43 ± 3.1	50.25 ± 1.2
	30.48 ± 1.6	144.03 ± 0.6
Physical Mixture GLZ	103.1 ± 0.9	54.32 ± 2.4
	38.80 ± 0.8	153.14 ± 1.3
Raw GLZ	131.3 ± 1.0	168.72 ± 0.9
St. MG	--	--
HPC	--	--
HPMCAS	--	--
PEG 4000	317.4 ± 2.2	61.35 ± 0.9

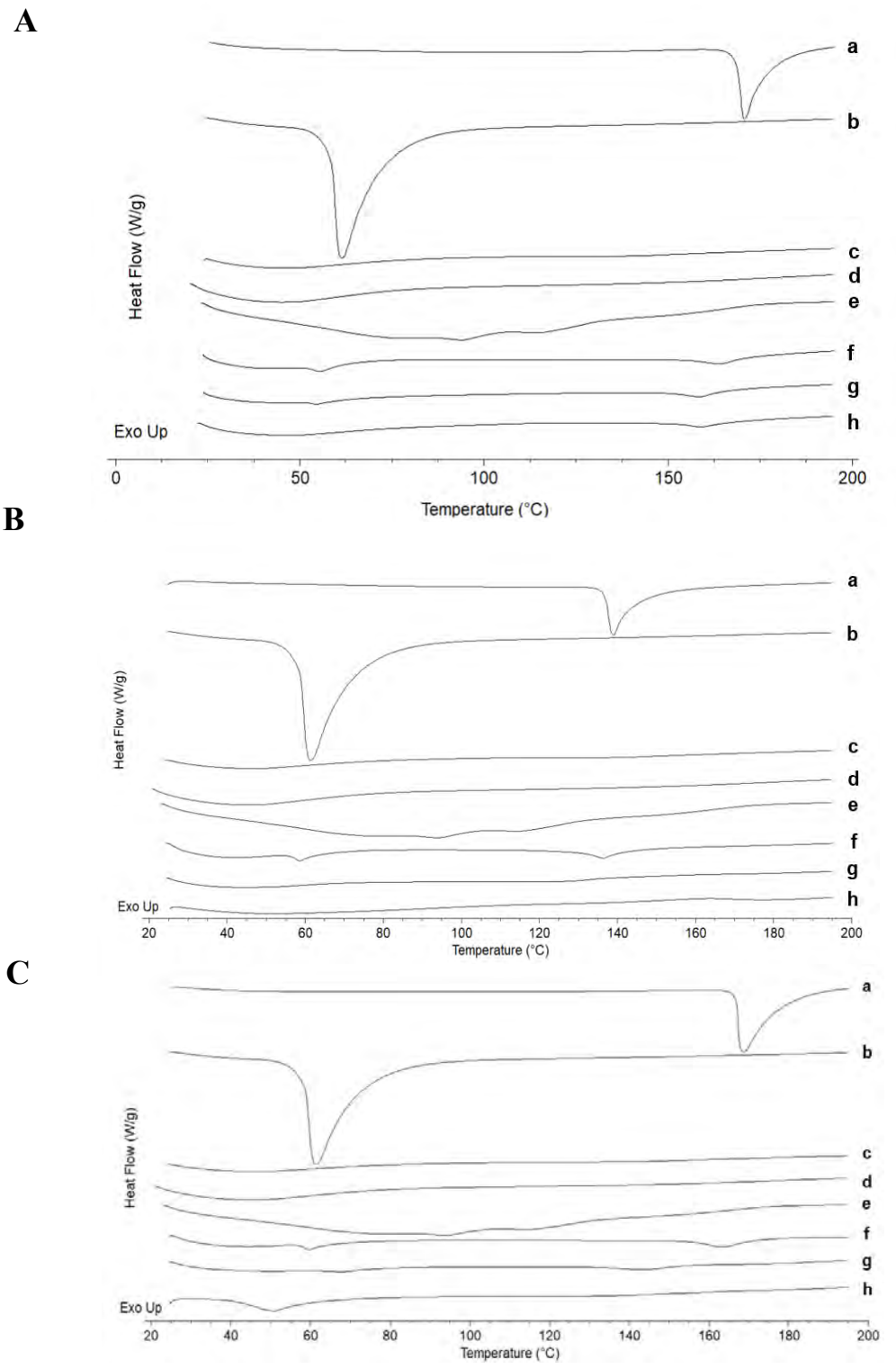

Figure 5. **DSC thermograms for (A) NFD, (B) SMV, (C) GLZ**. Key: (a) Unprocessed API, (b) Unprocessed PEG 4000, (c) Unprocessed HPMC, (d) Unprocessed HPC, (e) Unprocessed magnesium stearate, (f) Physical mixture, (g) API filament, and (h) API printed tablet.

3.3. Dissolution studies

3D printed NFD tablet showed a sustained drug release over a 24 h period. Compared to Adalat Oros, the commercially available formulation, the overall release from the 3D printed NFD tablet was significantly higher ($p < 0.05$) from 90 min up to 240 min. Adalat Oros showed a zero-order release as previously described [23] while NDF printed tablet followed a Korsmeyyer-Peppas kinetic in SIF (Fig. 6A). Adalat Oros is an osmotic tablet consisting of a NaCl compartment separated from the NFD compartment formulated with hypromellose and hydroxypropyl cellulose and PEG. The tablet is coated with a semipermeable membrane made of cellulose acetate that upon contact with aqueous media led to swelling of the NaCL compartment pushing the NFD to come out through a millimetric pore located on the surface [32]. This technology allows for a tune drug release over 24 h. In the case of the 3D printed NFD tablet, the matrix did not disintegrate, maintaining its shape and visually observing like a gel-surrounded structure modulating the release over time. The gel diffusion barrier allowed a controlled drug release over 24 h, but resulted in higher variability at later time points when the tablet lost the overall structure. ~~The release occurred by the slow erosion of the surface in contact with the aqueous media.~~

In the case of the SMV, the release was significantly ($p < 0.05$) more pronounced than the commercial tablet resulting in 80% drug dissolved after 4 h (Figure 6B). This faster release can be attributed to the amorphous nature of the drug within the excipient matrix. SMV is a prodrug activated by first-pass hepatic metabolism to a hydroxy acid metabolite which has a half-life of 1-2 h that inhibits the HMG CoA reductase limiting cholesterol synthesis at night [33]. This faster-release profile also fitting a Korsmeyer-Peppas kinetic is more suitable for SMV considering its limited half-life and its window of action.

Regarding the GLZ, no release was observed for the commercial formulation during the first two hours ~~followed by a zero-order kinetic release~~. However, the 3D printed tablet showed a faster onset of release even at acidic pH after 60 min which can be advantageous to control postprandial glycemia. After 180 min, the release profile was sustained over 24 h following also a Korspmeyyer-Peppas kinetic profile. The release profile of the polypill containing NFD, SMV, and GLZ at the same doses as the single API tablets followed a similar trend but with several differences. The release profile of SMV was slower and more sustained avoiding the initial burst effect observed in the 3D printed tablet with a single API. In the case of the

GLZ, the release profile from the polypill was also delayed up to 120 min. However, the release was sustained over time during 24 h.

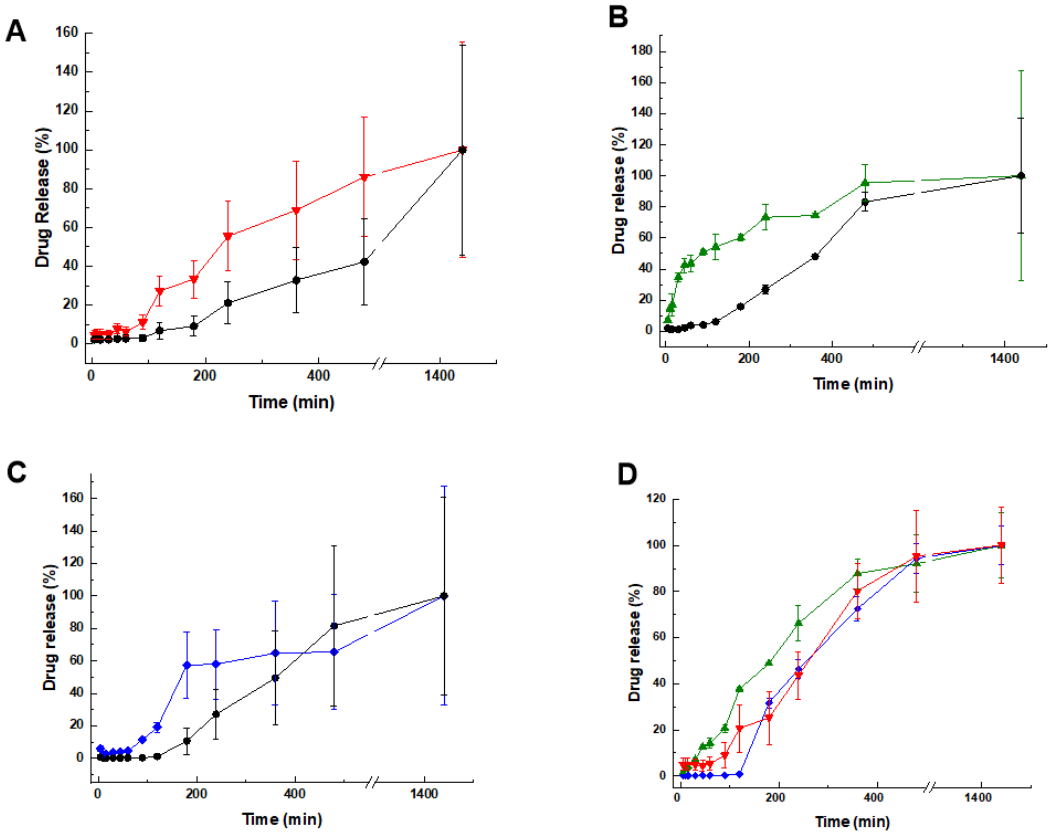

Figure 6. **Dissolution profile for the 3D printed tablets compared to commercially available formulations**. (A) nifedipine (NFD), (B) simvastatin (SMV), (C) gliclazide (GLZ), (D) 3D Polypill. Key: Commercial tablets include Adalat Oros, Simvastatin Normon and Gliclazide Cinfa (black) (–●–), NFD (red) (–▼–), SMV (green) (–▲–), GLZ (blue) (–◆–).

Hansen solubility parameters were calculated to understand the likelihood fof interaction between the drug and the excipients used. Values are reported in Table 3.

Table 3. Hansen solubility parameters (MPa)$^{1/2}$. *values obtained from: [26].

Molecule	δ_d	δ_p	δ_h	δ_t
NFD	16.58	2.38	7.41	18.3
SMV	22.47	3.11	9.40	24.6
GLZ	22.92	9.78	10.29	27.0
PEG	17.78	11.11	9.13	22.9
HPC	17.00	6.23	23.29	29.5
HPMCAS*	19.4	14.6	21.9	32.7

4. Discussion

The formation of amorphous solid dispersions (ASD) has varied amongst the three different drugs. During HME coupled with FDM, drugs undergo two cycles of intimate contact between drug and excipients. The selection of the excipients as well as the manufacturing conditions are key to ensure the successful formation of ASD. Hydrogen bonding interactions between API and polymers allow the amorphization of the drug inhibiting or delaying the crystallization process and ideally increasing the dissolution properties and oral bioavailability. Drugs selected for this study have a logP of 2.5, 4.7, and 2.6 for NFD, SMV, and GLZ respectively [34]. The HSP for the three drugs varied from 18.3 for NFD to 27.0 for GLZ (Table 3). HSPs were calculated as an indication of the miscibility of the API and excipients. The total solubility parameter, δ_t, is a measure of the attractive intermolecular forces in the material and hence, materials with similar δ_t, are considered miscible or one can dissolve in the other. Taking into account the percentage used for each of the excipients for filament manufacturing, the average δ_t for the excipient mixture was $27.3^{0.5}$. Based on differences found between the API δt, and the excipient mixture δt, it is evident to justify why the GLZ and SMV were amorphized within the 3D tablets but not the NFD. Also, the extrusion and printing parameters are crucial to ensure intimate contact between API and the excipient mixture. Even though GLZ has the closest δt to the excipient mixture δt, the drug amorphization only occurred after the 3D printing but not during the extrusion process. This can be explained due to the lower temperature utilized during the process (25ºC below the melting point of the drug). Higher temperatures were not used as drug degradation was too pronounced.

In our study, the importance of selecting suitable manufacturing parameters as well as adequate excipients miscible with the APIs has been illustrated. HSP can be used as a predictor tool to evaluate drug-polymer miscibility.

The greater miscibility between SMV and the excipient mixture resulted in a 3D ASD tablet with a faster dissolution profile compared to NFD and GLZ but also to the commercial SMV tablet formulation. In less than 6 h, all API was fully dissolved while NFD and GLZ took longer times, closer to 24 h to reach 100% drug release. This release profile was carefully designed for a night intake polypill for the treatment of metabolic syndrome. SMV acts by inhibiting the enzyme HMG CoA reductase that regulates the synthesis of cholesterol in the

liver. Cholesterol is synthesised when dietary intake is at its lowest, and hence, clinicians recommend the intake of SMV at night [35]. However, several meta-analyses have quantitated the excess risk of cardiovascular events in the hours around and just after awakening existing a 40% higher risk of heart attack, 29% increased risk of cardiac death and 49% increased risk of stroke between 6 am and noon [36]. Based on this, it is key that night antihypertensive pills have a prolonged effect overnight to reduce the risk of cardiovascular events in the morning. The 3D printed NFD tablet exhibited a 24 h release making it useful for this purpose. Regarding the GLZ, the 3D printed tablet showed a burst effect (60% release over 3 h), followed by a 24 h sustained release. This makes it suitable to prevent postprandrial glycemia and maintain constant levels overnight. However, further in vitro-in vivo correlation studies should be performed to demonstrate this hypothesis.

During the last decade, 3D printing has demonstrated to be a powerful tool in the design of formulations as well as many other applications such as microfluidics or tissue engineering [37-39]. In pharmaceutics, 3D printing has shown great versatility to modulate drug release profiles within solid dosage forms. There are hundreds of publications regarding a single API 3D printed tablet using different 3D printing techniques. However, manufacturing of 3D printed polypills for metabolic syndrome containing three or more APIs is challenging.

Using FDM, a three-drug polypill has been designed containing captopril, an angiotensin-converting enzyme (ACE), glipizide, a hypoglycemic drug, and nifedipine, a calcium antagonist [40]. Captopril had a zero-order release due to the addition of mannitol as an osmotic agent while glipizide and nifedipine were embedded in a hydrophilic matrix of hydroxypropyl methylcellulose with a first-order release [8]. A five-in-one-dose combination polypill was successfully printed using another 3D printing technique, pressure-assisted microsyringes or semisolid extrusion [14]. The tablet containing aspirin as an antiplatelet and hydrochlorothiazide as a diuretic combined with sodium starch glycolate and polyvinylpyrrolidone K30 as disintegrant and binder in the immediate release layer, and atenolol as a beta-blocker, ramipril as an ACE inhibitor, and pravastatin as a 3-hydroxy-3-methylglutaryl–coenzyme in the sustained release layer which was physically separated from the immediate release layer by a hydrophobic cellulose acetate shell. The main disadvantage of this technique is the post-processing step to dry the solid dosage forms which can last several hours and also the risk of solvent traces left in the tablets. Stereolithography also has

been used to manufacture polypills. A six-drug tablet was printed with paracetamol, caffeine, aspirin, naproxen, chloramphenicol, and prednisolone [13]. However, for successful printing using this technique is necessary to employ polimerizable resins and photoinitiators which may be toxic for humans especially when used in chronic diseases such as metabolic syndrome [8].

Based on the current state-of-the-art for manufacturing 3D printed polypills, FDM coupled with HME has shown the most promising results for clinical implementation taking into account that excipients used are of pharmaceutical grade already approved for use in humans and there is no risk of solvent traces in the final dosage formulations. However, further research is required to facilitate the translation from bench to clinic, especially regarding the fabrication of filaments to understand which API-polymer composition is more suitable for the required release profile and patient's needs.

5. Conclusion

In this work, the transformation of FDC polypills into dynamic personalized doses for the treatment of metabolic syndrome has been demonstrated. FDM is a versatile technology that can be implemented in clinical practice if filaments with optimal printing characteristics are manufactured. HSP can be used as a predictor tool to evaluate the miscibility between the drug and the excipient mixture and the likelihood of amorphous solid dispersion formation to enhance oral bioavailability, which is especially important in poorly water-soluble drugs. The largest difference in HSP was exhibited between the NFD and the excipient mixture utilized for the manufacturing of filaments and 3D-printed tablets which can explain the partially crystalline nature of the drug in the final dosage form. Another interesting observation is the difference found between the release profile of the same drug in a single 3D printed tablet or the combination in a multi-layered polypill. The change in release profile between a single drug and a polypill was more pronounced in the SMV, exhibiting a significant delay when combined with the other two active pharmaceutical ingredients.

Acknowledges

This research was funded by Universidad Complutense de Madrid (910939) Formulacion y biodisponibilidad de nuevos medicamentos. This study has also been partially funded by the Ministry of Science and Innovation (award PID2021-126310OA-I00 to Dolores Serrano).

References

1. Oluwaseun, C., et al., *Potentialities of nanomaterials for the management and treatment of metabolic syndrome: A new insight.* Materials today advances, 2022. **13**: p. 100198.
2. Buchmann, N., et al., *Muscle Mass and Inflammation in Older Adults: Impact of the Metabolic Syndrome.* Gerontology, 2022. **68**(9): p. 989-998.
3. Zema, L., et al., *Three-Dimensional Printing of Medicinal Products and the Challenge of Personalized Therapy.* J Pharm Sci, 2017. **106**(7): p. 1697-1705.
4. Abrahams, E., *Right drug-right patient-right time: personalized medicine coalition.* Clin Transl Sci, 2008. **1**(1): p. 11-2.
5. Serrano, D.R., M.C. Terres, and A. Lalatsa, *Applications of 3D printing in cancer.* Journal of 3D printing in medicine, 2019. **2**(3).
6. Beer, N., et al., *Scenarios for 3D printing of personalized medicines - A case study.* Explor Res Clin Soc Pharm, 2021. **4**: p. 100073.
7. Konta, A.A., M. Garcia-Pina, and D.R. Serrano, *Personalised 3D Printed Medicines: Which Techniques and Polymers Are More Successful?* Bioengineering (Basel), 2017. **4**(4).
8. Serrano, D.R., et al., *3D Printing Technologies in Personalized Medicine, Nanomedicines, and Biopharmaceuticals.* Pharmaceutics, 2023. **15**(2).
9. Goh, O., et al., *Preferences of Healthcare Professionals on 3D-Printed Tablets: A Pilot Study.* Pharmaceutics, 2022. **14**(7).
10. Fernandez-Garcia, R., et al., *Oral Fixed-Dose Combination Pharmaceutical Products: Industrial Manufacturing Versus Personalized 3D Printing.* Pharm Res, 2020. **37**(7): p. 132.
11. Kara, A., et al., *3D Printing Technologies for Personalized Drug Delivery.* , in *Emerging Drug Delivery and Biomedical Engineering Technologies: Transforming Therapy*, D. Lamprou, Editor. 2023, CRC Press
12. Goh, W.J., et al., *3D printing of four-in-one oral polypill with multiple release profiles for personalized delivery of caffeine and vitamin B analogues.* Int J Pharm, 2021. **598**: p. 120360.
13. Robles-Martinez, P., et al., *3D Printing of a Multi-Layered Polypill Containing Six Drugs Using a Novel Stereolithographic Method.* Pharmaceutics, 2019. **11**(6).
14. Khaled, S.A., et al., *3D printing of five-in-one dose combination polypill with defined immediate and sustained release profiles.* J Control Release, 2015. **217**: p. 308-14.
15. Cerda, J.R., et al., *Personalised 3D Printed Medicines: Optimising Material Properties for Successful Passive Diffusion Loading of Filaments for Fused Deposition Modelling of Solid Dosage Forms.* Pharmaceutics, 2020. **12**(4).
16. Ayyoubi, S., et al., *3D printed spherical mini-tablets: Geometry versus composition effects in controlling dissolution from personalised solid dosage forms.* Int J Pharm, 2021. **597**: p. 120336.
17. Keikhosravi, N., et al., *Preparation and characterization of polypills containing aspirin and simvastatin using 3D printing technology for the prevention of cardiovascular diseases.* Drug Dev Ind Pharm, 2020. **46**(10): p. 1665-1675.
18. McDonagh, T., P. Belton, and S. Qi, *Manipulating drug release from 3D printed dual-drug loaded polypills using challenging polymer compositions.* Int J Pharm, 2023. **637**: p. 122895.
19. Pereira, B.C., et al., *'Temporary Plasticiser': A novel solution to fabricate 3D printed patient-centred cardiovascular 'Polypill' architectures.* Eur J Pharm Biopharm, 2019. **135**: p. 94-103.

20. Windolf, H., et al., *3D Printed Mini-Floating-Polypill for Parkinson's Disease: Combination of Levodopa, Benserazide, and Pramipexole in Various Dosing for Personalized Therapy.* Pharmaceutics, 2022. **14**(5).
21. Sadia, M., et al., *From 'fixed dose combinations' to 'a dynamic dose combiner': 3D printed bi-layer antihypertensive tablets.* Eur J Pharm Sci, 2018. **123**: p. 484-494.
22. Malebari, A.M., et al., *Development of Advanced 3D-Printed Solid Dosage Pediatric Formulations for HIV Treatment.* Pharmaceuticals (Basel), 2022. **15**(4).
23. Sanchez-Guirales, S.A., et al., *Understanding Direct Powder Extrusion for Fabrication of 3D Printed Personalised Medicines: A Case Study for Nifedipine Minitablets.* Pharmaceutics, 2021. **13**(10).
24. Walsh, D., et al., *Engineering of pharmaceutical cocrystals in an excipient matrix: Spray drying versus hot melt extrusion.* Int J Pharm, 2018. **551**(1-2): p. 241-256.
25. Walsh, D., et al., *Production of cocrystals in an excipient matrix by spray drying.* Int J Pharm, 2018. **536**(1): p. 467-477.
26. Chen, X., et al., *Solubility Improvement of Progesterone from Solid Dispersions Prepared by Solvent Evaporation and Co-milling.* Polymers (Basel), 2020. **12**(4).
27. Daniela Amaral Silva, et al., *Update on Gastrointestinal Biorelevant Media and Physiologically Relevant Dissolution Conditions.* 2022.
28. (USP), u.s.p. *chapter No, <711> Dissolution; Volume 41. Available online: www.usppf.com (accessed on 14 March 2023).*
29. Muselik, J., et al., *A Critical Overview of FDA and EMA Statistical Methods to Compare In Vitro Drug Dissolution Profiles of Pharmaceutical Products.* Pharmaceutics, 2021. **13**(10).
30. Serrano, D.R., et al., *Cocrystal habit engineering to improve drug dissolution and alter derived powder properties.* J Pharm Pharmacol, 2016. **68**(5): p. 665-77.
31. Ilyes, K., et al., *The applicability of pharmaceutical polymeric blends for the fused deposition modelling (FDM) 3D technique: Material considerations-printability-process modulation, with consecutive effects on in vitro release, stability and degradation.* Eur J Pharm Sci, 2019. **129**: p. 110-123.
32. cima. *Adalat Oros 30 mg, comprimidos de liberación prolongada (nifedipino)*. 2020; Available from: https://cima.aemps.es/cima/dochtml/p/59538/P_59538.html.
33. Waller, D.G. and A.P. Sampson, *Lipid disorders*, in *Medical Pharmacology and Therapeutics*. 2018. p. 547-557.
34. *Durg bank datase. Available at: https://go.drugbank.com/ Accessed date: 16 April 2023.*
35. Wallace, A., D. Chinn, and G. Rubin, *Taking simvastatin in the morning compared with in the evening: randomised controlled trial.* BMJ, 2003. **327**(7418): p. 788.
36. Elliot, W.J., *Cyclic and circadian variations in cardiovascular events.* Am J Hypertens, 2001. **14**(9 Pt 2): p. 291S-295S.
37. Kara, A., et al., *Engineering 3D Printed Microfluidic Chips for the Fabrication of Nanomedicines.* Pharmaceutics, 2021. **13**(12).
38. Osouli-Bostanabad, K., et al., *Microfluidic Manufacture of Lipid-Based Nanomedicines.* Pharmaceutics, 2022. **14**(9).
39. Yuste, I., et al., *Mimicking bone microenvironment: 2D and 3D in vitro models of human osteoblasts.* Pharmacol Res, 2021. **169**: p. 105626.
40. Khaled, S.A., et al., *3D printing of tablets containing multiple drugs with defined release profiles.* Int J Pharm, 2015. **494**(2): p. 643-650.